Stem Cells, 2023, **41**, 862–876
https://doi.org/10.1093/stmcls/sxad047
Advance access publication 15 June 2023
Original Research

ZIC1 Dictates Osteogenesis Versus Adipogenesis in Human Mesenchymal Progenitor Cells Via a Hedgehog Dependent Mechanism

Neelima Thottappillil[1], Mario A. Gomez-Salazar[1], Mingxin Xu[1], Qizhi Qin[1], Xin Xing[1], Jiajia Xu[1], Kristen Broderick[2], Ji-Hye Yea[1], Mary Archer[1], Ginny Ching-Yun Hsu[3], Bruno Péault[4,5], Aaron W. James[*,1]

[1]Department of Pathology, Johns Hopkins University, Baltimore, MD, USA
[2]Department of Plastic Surgery, Johns Hopkins University, Baltimore, MD, USA
[3]Department of Orthodontics, Oregon Health and Science University, Portland, OR, USA
[4]Department of Orthopaedic Surgery and Orthopaedic Hospital Research Center, UCLA, Los Angeles, CA, USA
[5]Center for Cardiovascular Science, University of Edinburgh, Edinburgh, UK

*Corresponding author: Aaron W. James, Department of Pathology, Johns Hopkins University, Ross Research Building, Room 524A, 720 Rutland Avenue, Baltimore, MD 21205, USA. Tel: +1 410 502 4143; Fax: +1 410 955 0394; Email: awjames@jhu.edu

Abstract

Numerous intrinsic factors regulate mesenchymal progenitor commitment to a specific cell fate, such as osteogenic or adipogenic lineages. Identification and modulation of novel intrinsic regulatory factors represent an opportunity to harness the regenerative potential of mesenchymal progenitors. In the present study, the transcription factor (TF) *ZIC1* was identified to be differentially expressed among adipose compared with skeletal-derived mesenchymal progenitor cells. We observed that *ZIC1* overexpression in human mesenchymal progenitors promotes osteogenesis and prevents adipogenesis. *ZIC1* knockdown demonstrated the converse effects on cell differentiation. *ZIC1* misexpression was associated with altered Hedgehog signaling, and the Hedgehog antagonist cyclopamine reversed the osteo/adipogenic differentiation alterations associated with *ZIC1* overexpression. Finally, human mesenchymal progenitor cells with or without *ZIC1* overexpression were implanted in an ossicle assay in NOD-SCID *gamma* mice. *ZIC1* overexpression led to significantly increased ossicle formation in comparison to the control, as assessed by radiographic and histologic measures. Together, these data suggest that *ZIC1* represents a TF at the center of osteo/adipogenic cell fate determinations—findings that have relevance in the fields of stem cell biology and therapeutic regenerative medicine.

Key words: ZIC1; osteogenesis; adipogenesis; mesenchymal progenitor cells; mesenchymal stem cell; pericytes; bone tissue engineering; Sonic Hedgehog signaling; ossicle formation.

Graphical Abstract

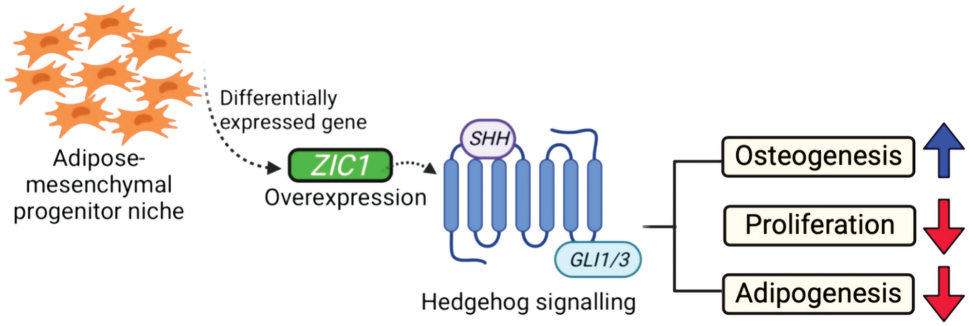

Received: 3 January 2023; Accepted: 23 May 2023.

Significance Statement

Identification of novel transcription factors regulating lineage commitment in mesenchymal progenitor cells is necessary to understand niche-specific attributes of stem cells. Moreover, these intrinsic factors could be modulated to assist differentiation of progenitor cells toward lineages of therapeutic interest. Here, overexpression of the *ZIC1* transcription factor forced progenitor cells to make more bone at the expense of fat. This modulation acts predominantly through a Hedgehog-dependent mechanism. The present findings provide important insight into an intrinsic factor and its mechanism that regulate bone formation, which could be further leveraged for tissue (re) generation.

Introduction

Autologous stem cell-based tissue regeneration therapies hold great promise to address the significant biomedical burden related to bone pathologies.[1] The multilineage differentiation potential of mesenchymal stem cells can assist in the treatment of bone diseases.[2-4] However, the inconsistent performance of mesenchymal stem cells for bone tissue regeneration *in vivo* poses a significant impediment to clinical translation.[5,6] Consistent cell-based bone tissue regeneration requires an improved understanding of progenitor cell subpopulations and defined niche-specific regeneration attributes.[7] Our group has focused on perivascular mesenchymal progenitor cells,[1] including their bone-forming efficacy,[8,9] heterogeneity,[10,11] and intrinsic and extrinsic regulatory factors.[11,12]

Adipose-derived mesenchymal progenitor cells including perivascular CD146$^+$ pericytes show tissue-specific functional characteristics. In our previous studies, we observed that human skeletal pericytes have a natural predisposition to form more bone in culture and ossify after xenotransplantation.[13] In another study, pericytes derived from the human kidney secreted functionally active renin, evidencing tissue-specific functions.[14] These results support the notion that pericytes are inclined to mature into the lineage supported by the microenvironment from which they are isolated, yet also retain their multipotency across contexts.[9]

However, we observed previously that adipose tissue-derived *CXCR4*$^+$CD146$^+$ human pericytes, which also maintain stem-like properties, exhibit a skeletogenic rather than adipocytic nature.[15] This can be particularly attributed to specific genes and signaling pathways that maintain tissue-specific potential.[12,16] An inverse correlation is well known to exist in the processes of adipogenesis and osteogenesis from mesenchymal progenitor cells.[5,17,18] The transdifferentiating potential of adipose-derived stem cells to an osteoblastic lineage can be reasoned by the influence of certain signaling pathway that predominantly mediates osteogenic fate commitment of specific subsets of adipose progenitors.[19,20] Thus, the lineage commitment of stem cells depends on the tight regulatory activities of transcription factors (TFs) in response to external signals received from the cell microenvironment.[21] Overexpressing TFs such as *MAFF*, *BATF3*, and *MXD4* could inhibit adipogenesis from human adipose-derived stem cells.[22] Thereby, modulating the transcriptional regulation could commit stem cells to differentiate to a specific lineage different from its native niche. Further identification of these TFs is necessary to understand the intricacies of progenitor lineage commitment. Moreover, forced misexpression of these TFs may alter the osteo-adipogenic balance of mesenchymal progenitor cells, which can be used for therapeutic tissue regeneration.[23-26]

In the present study, *ZIC1* was identified as a TF differentially expressed across human pericytes derived from different tissue sources. Several studies have implicated *ZIC1* in vertebral skeletal development, and mutations in the *ZIC1* gene cause skeletal pathologies.[27-29] The role of *ZIC1* in the modulation of human stem cell fate was investigated. Overexpression of *ZIC1* in adipose mesenchymal progenitors led to increased osteogenesis both *in vitro* and *in vivo*, which could be further leveraged in bone regeneration therapies.

Materials and Methods

Isolation and Culture of Human Adipose-Derived Progenitor Cells, CD146$^+$ Pericytes and Human Periosteal CD146$^+$ Pericytes

All human adipose tissue fat and bone samples were obtained from adult patient donors under Institutional Review Board (IRB) approval (#00119905) at Johns Hopkins University (JHU) with a waiver of informed consent (Supplementary Table S1). Human adipose-derived mesenchymal progenitor cells (hASCs) and pericytes were isolated according to previously reported protocols.[15,30] Briefly, to isolate adipose-derived mesenchymal progenitor cells and pericytes, lipoaspirate from human liposuction was washed in phosphate-buffered saline (PBS) and centrifuged to separate the fat from the oil and liquid phases. Fat was mixed with 1 mg/mL Type II collagenase (Sigma Aldrich, St Louis, MO, USA) in DMEM + 0.5% bovine serum albumin (BSA) (Cohn Fraction V A7906; Sigma) and digested for 45 minutes at 37 °C in a shaking water bath (150 *g*). The digested adipose tissue was then centrifuged, and the pellet was resuspended in PBS with 2% BSA. This was serially filtered at 100 μM and 70 μM. After centrifugation, the pellet was further incubated in red cell lysis buffer (155 mM NH4Cl, 10 mM KHCO3, and 0.1 mM EDTA) at RT for 10 minutes. After centrifugation, the stromal vascular fraction (SVF) was resuspended in PBS + 2% BSA and filtered at 40 μM. The cell suspension was further counted for live cells using trypan blue staining. A part of the cell suspension was mixed with warm Alpha MEM medium + 15% FBS + 1% antibiotic/antimycotic and seeded directly to culture plates to obtain adherent mesenchymal cells. The other part of the cells was further processed for sorting, using a mixture of the following directly conjugated antibodies: anti-CD31-APC-cy7 (1:100), anti-CD45-APC-cy7 (1:30), anti-CD34-APC (1:30), and anti-CD146-fluorescein isothiocyanate (1:100) (Supplementary Table S2). All incubations were performed at 4 °C for 15 minutes. After incubation, cells were sorted as CD146$^+$CD34$^-$CD31$^-$CD45$^-$ pericytes on a MoFlo XDP flow cytometer (Beckman Coulter, IN, USA) and analyzed with Summit Software (PrismHR, MA, USA). The collected cells were seeded onto 96-well plates coated with 0.2% gelatin. The cells were cultured in EGM-2 medium (Lonza). The medium was replenished the next day and changed every 3 days thereafter. Similarly, human periosteal pericytes were isolated as previously reported.[15] Briefly, long

bones, either tibia or femur (obtained from nonneoplastic resections), were stored for <48 hours at 4 °C before processing. Using a periosteal elevator, the periosteum was detached and dissected. Periosteal tissue was further minced and digested with 1 mg/mL type I collagenase in DMEM for 90 minutes under agitation at 37 °C. After centrifugation, the cell pellet was resuspended in red blood cell lysis buffer and incubated at 37 °C for 5 minutes. After filtration using 40 μM filters, the cell pellet was stained as described above and run on a MoFlo XDP flow cytometer to collect periosteal pericytes. Pericytes were seeded on 96-well plates and cultured until confluence.

Microarray Analysis

The transcriptomes of adipose tissue were examined by analyzing a microarray previously published by our group.[15] Here, total RNA from FACS-derived adipose and periosteal human CD146$^+$ pericytes was isolated by Trizol (Life Technologies Corporation). Purified RNA samples were sent to the JHMI Transcriptomics and Deep Sequencing Core (JHU, Baltimore, MD, USA) for analysis using an Affymetrix Clariom D microarray (Affymetrix, Santa Clara, CA, USA). Expression data were deposited in the Gene Expression Omnibus (GEO) repository (GSE125545).[15] Data analyses were performed using Spotfire DecisionSite software package. Differential expression of TFs was detected by querying the micro array data to the known human TFs and using as a threshold a P value < .05 and Log_2 (fold change) ≥ 1. Volcano plot was created with the R package Enhanced Volcano (Bioconductor). Heatmaps were created with the R package Pheatmap.

Immunohistochemistry and Microscopy

For immunohistochemistry, human fat tissue was snap-frozen and embedded in optimal cutting temperature medium (Sakura, Torrance, CA) and cryo-sectioned at 30 μM thickness. Deidentified human periosteum samples were obtained from our surgical pathology archives (Johns Hopkins University) under IRB approval and informed consent. The bone samples were decalcified in 14% EDTA for 8 weeks before sectioning, embedded in OCT medium and cryo-sectioned at 20 μM thickness. For immunofluorescence staining, slides were initially warmed at 55 °C, and sections were fixed with a 4% paraformaldehyde solution for 10 minutes. Next, slides were washed with PBS 2 times each for 5 minutes and permeabilized with 0.1% Triton X-100 in PBS. The sections were blocked with Superblock (Thermo Fisher Scientific) and further with 10% donkey serum in PBS for 1 hour. The primary antibodies (Supplementary Table S2) were added to corresponding sections and incubated in a moist chamber overnight at 4 °C. After washing, secondary antibodies were added (1:500) and incubated at room temperature for 1 hour. Next, sections were counterstained with DAPI mounting medium (Vector Laboratories, Burlingame, CA) and examined under a Zeiss LSM800 GaAsP single-point laser scanning microscope.

Small Interfering RNA (siRNA) Transfection for *ZIC1* Knockdown

Knockdown of *ZIC1* was performed using Silencer Select chemically synthesized siRNA (Thermo Fisher Scientific, Cat# 4392420, Ref_seq NM_003412.3, s14995). The control used was Select Negative Control No. 1 siRNA (Thermo, Silencer select, Cat#. 4390843). Cells were seeded at a density of 5 × 10^4 cells per well. At 80% confluence, growth medium was replaced with OptiMEM medium (Thermo Fisher). Transfection was performed using TransIT-X2 siRNA Transfection Reagent (Mirus Bio) and 150 pm *ZIC1* siRNA or scramble siRNA. Medium was changed into complete growth medium 2 hours posttransfection. The efficiency of the knockdown was validated using qRT-PCR. See Supplementary Table S3 for primers used.

Plasmid Transfection for *ZIC1* Overexpression

ZIC1 was overexpressed using a human *ZIC1* open reading frame (ORF) mammalian expression plasmid (RG220233, Origene, Rockville, MD). Cells were seeded and maintained to reach 80% confluence. Lentivirus-mediated plasmid transfection was performed for *ZIC1* overexpression. 1 μg of *ZIC1* plasmid and empty lentiviral vehicle were transfected using TransIT-X2 Dynamic delivery system (Mirus Bio, USA) according to the manufacturer's protocol. At 2 hours posttransfection, the medium was changed to complete growth medium. qRT-PCR was used to measure *ZIC1* gene expression 48 hours posttransfection.

Culture of Osteosarcoma Cell Line

To verify findings in primary cells, the Saos-2 human osteosarcoma cell line was purchased from the American Type Culture Collection (ATCC HTB-85). Cells were grown and maintained in Alpha MEM medium with 10% FBS and 1% penicillin/streptomycin. Cells were transfected with *ZIC1* plasmid or vehicle control as described earlier.

Cell Proliferation Assays

Proliferation assays were performed in 96-well plates (2 × 10^3 cells/well) and measured for up to 48 hours using the CellTiter96 Aqueous One Solution Cell Proliferation Assay kit (MTS, G358A; Promega, Madison, WI). Briefly, 10 μL of MTS solution was added to each well and incubated for 3 hours at 37 °C. The absorbance was assayed at 490 nm using an Epoch microspectrophotometer (Bio-Tek, Winooski, VT).

Western Blot

After 48 hours of either *ZIC1* knockdown or overexpression, cells were lysed in RIPA buffer (Thermo Fisher Scientific, USA) with added protease inhibitor cocktail (Cell Signalling Technology, Danvers, MA). Total protein concentration was determined by the BCA assay kit (Thermo Fisher Scientific, USA). Proteins were separated by SDS-PAGE and transferred to a nitrocellulose membrane. The membranes were incubated with antibodies overnight (1:1000). The secondary antibody (1:1000) was added next day and visualized as previously reported.[31] Antibodies used are listed in Supplemental Table S2. Band intensity is calculated using ImageJ (NIH, USA) software and normalized with GAPDH.

Adipogenic Differentiation and Quantification

Transfected cells were plated at a density of 2 × 10^5 cells per well. Basal medium was replaced with adipogenic differentiation medium consisting of DMEM, 10% FBS, 1% indomethacin, 0.5 mM isobutyl methyl xanthine, and 1 mmol·L^{-1} dexamethasone and 200 mM insulin every other day of

differentiation. Oil red O staining was performed after 10 days of differentiation.[3,14,17] Cells were washed with PBS and fixed with 4% PFA for 15 minutes. After fixation, cells were washed with water and 500 µL of Oil red O staining solution, performed for 30 minutes at 37 °C. Following incubation, cells were washed with 60% isopropanol, followed by microscopy. After imaging, the Oil Red O stain was extracted with 100% isopropanol for 5 minutes followed by absorbance at 548 nm for quantification. All experiments were performed with n = 3 human samples per anatomic depot and in triplicate wells (biologic and technical triplicates).

Osteogenic Differentiation and Quantification

The transfected cells were plated at a density of 2×10^5 cells per well. Osteogenic differentiation medium (ODM) consisted of DMEM, 10% FBS, 1% a with 10 mmol·L^{-1} β-glycerophosphate, 50 µmol·L^{-1} ascorbic acid, and 1 mmol·L^{-1} dexamethasone. Medium was changed every other day during differentiation

For ALP and Alizarin Red (AR) staining, cells were washed with PBS and fixed with 4% PFA at 10 to 14 days of differentiation. Next, cells were stained with diazonium salt with 4% naphthol AS-MX phosphate alkaline solution at RT for 15 minutes for alkaline phosphatase detection, or with 2% AR solution at RT for 10 minutes for bone nodule staining microscopic images were obtained using a Leica (LASX9) camera, and whole well pictures were captured using an Olympus Epson scanner (Los Angeles, CA, USA). For quantification, bone nodules were dissolved in 0.1 N sodium hydroxide and quantified using an Epoch microspectrophotometer (BioTek, Winooski, VT, USA) by an absorbance at 548 nm. All experiments were performed with n = 3 human samples per anatomic depot and in triplicate wells (biologic and technical triplicates).

Quantitative (q)RT-PCR

Gene expression after *ZIC1* knockdown and overexpression were analyzed by qRT-PCR. Total RNA was extracted using geneElute single cell RNA isolation kit (Sigma Aldrich, USA). From the total RNA, 1 µg of RNA was reverse transcribed to first-strand complementary deoxyribonucleic acid (cDNA) synthesis using the iScript cDNA Synthesis Kit (Bio-Rad) to a final volume of 20 µL. The reverse transcription was performed at 25 °C for 5 minutes, followed by 46 °C for 20 minutes and 95 °C for 1 minute. For qRT-PCR, the reaction was performed using Power SYBR Green master mix (Applied Biosystems) and QuantStudio 5 Real-Time PCR system instrument (Thermo Fisher Scientific, Waltham, MA). qRT-PCR was performed using 384-well optical plates at 95 °C for 10 minutes, followed by 40 cycles at 95 °C for 15 seconds and at 60 °C for 60 seconds. The fold change of each gene was calculated using the $2^{-\Delta\Delta Ct}$ method after normalizing to expression level of the housekeeping gene GAPDH and considering the untreated control expression as 1.

Cyclopamine Drug Treatment

ZIC1 overexpressing cells were treated with the Hedgehog antagonist cyclopamine. Based on preliminary cytotoxicity assays of the drug, 5 µM concentration was used. After transfection with *ZIC1*, the drug was added along with osteogenic medium both in vector control and *ZIC1* overexpression conditions. The drug containing medium was changed every other day for 14 days.

Immunocytochemistry and Imaging

Cells after *ZIC1* overexpression were seeded on 8-well chamber slides. After culturing for 48 hours, cells were washed with PBS and fixed with 4% PFA. Cells were permeabilized with 0.1% Triton X-100 and blocked with super block (Invitrogen). Cells were incubated with primary antibodies overnight at 4 °C for ZIC1 (1:100) and GLI3 (1:50). Following this, a corresponding secondary antibody (1:500) was added and incubated for 1 hour. Cells were counterstained with DAPI mounting medium and imaged under a Zeiss LSM 800 confocal microscope, and images were processed with ZEN blue software (Zeiss, USA).

Animal Care and Subcutaneous Ossicle Formation

All animals were housed, and experiments performed in accordance with the approved protocol of the Animal Care and Use Committee at Johns Hopkins University (JHU) and institutional guidelines. Ten-week-old male NOD-SCID *gamma* mice (strain #: 00557, NOD.Cg-*Prkdc*^{scid} *Il2rg*^{tm1Wjl}/SzJ RRID:BCBC_4142 Jackson Laboratory, USA) were used. Implantation was performed as per previously published protocols.[13] 3×10^6 cells/mL *ZIC1* overexpressing cells or lentiviral vehicle control-treated cells were trypsinised and mixed with a pre-weighed hydroxyapatite/β-tricalcium phosphate (HA/β-TCP) mixture (w/w = 6:4, total weight 45 mg) (Zimmer Dental Inc, Carlsbad, CA) and incubated at 37 °C for 3 hours. To assess for cell adhesion, the cells remaining in the medium after scaffold implantation were counted (Thermo Ficher Countess II, Supplementary Fig. S4). The mixture was implanted into the dorsal surface of mice subcutaneously (n = 6). Briefly, after anesthesia and analgesia, a patch of hair was removed from the skin surface with clippers. The surface of the skin was wiped with betadine. Two implants per mouse were placed on opposite sides (one side corresponding to *ZIC1* overexpression and the other side to lentiviral control). Furthermore, 15-mm incisions were made on the dorsal skin, and cavity was exposed. The HA/β-TCP granules with cells were scooped with a sterile spatula and carefully placed far laterally beneath the skin and far from the midline. Postimplantation X-ray images were taken to confirm the implant position (Supplementary Fig. S5). The incision was then closed using a monofilament suture in a simple interrupted fashion.

DEXA Scanning and Analysis

Implanted mice underwent dual absorption energy X-ray analysis at 4, 8, and 12 weeks. The total bone mineral density (BMD) of the implant was calculated by assessing arbitrary tissue regions of interest on the implants (n = 3 regions per implant).

MicroCT Imaging and Analysis

After 12 weeks, explants were collected and fixed with 4% (w/v) paraformaldehyde for 24 hours. Samples were then subjected to *ex vivo* high-resolution microCT imaging (Skyscan 1275, Bruker MicroCT, Belgium). Scanning parameter settings included using 1 mm of an aluminum filter with an anode current of 153 µA and voltage of 65 kV. The exposure time was 218 ms with 0.3° rotation stem and frame

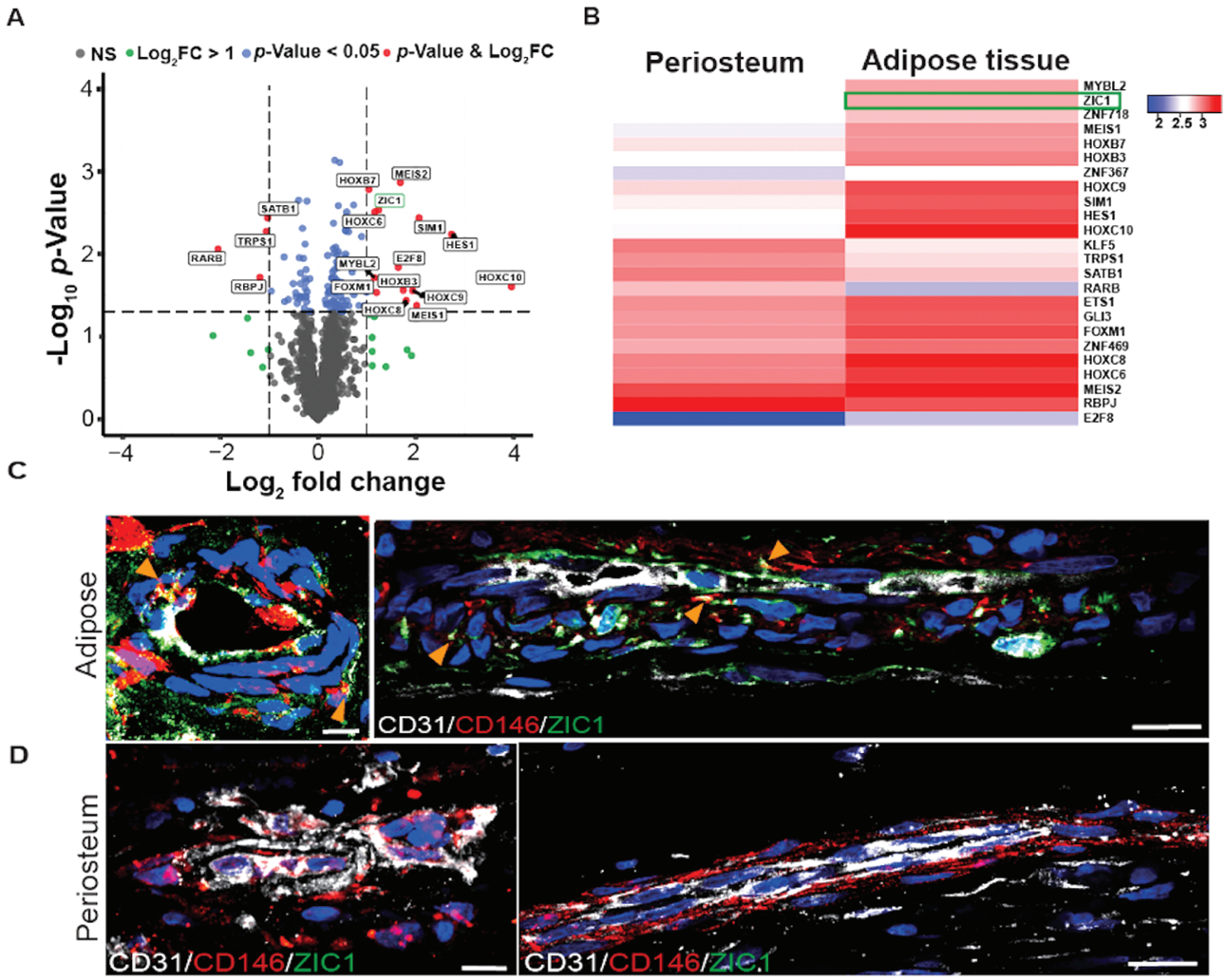

Figure 1. *ZIC1* is differentially expressed in adipose-derived progenitor cells in comparison to skeletal perivascular progenitor cells. Microarray analysis and immunofluorescence staining showing heightened *ZIC1* gene expression among adipose tissue pericytes. (**A**) Volcano plot of microarray data among CD146$^+$ adipose-derived or periosteal-derived human pericytes. Reanalysis from reference[15] *ZIC1* transcript enrichment among adipose-derived pericytes is shown (green box). (**B**) Heat map of differentially expressed transcription factors (TFs) among human pericytes from adipose or periosteal tissue. (**C**) Immunostaining of *ZIC1* (green, yellow arrowheads) co-expressed with the pericyte marker CD146 (red) within human blood vessels in subcutaneous adipose tissue. CD31 (white) highlights endothelium. (**D**) Immunostaining of ZIC1, CD146, and CD31 in blood vessels within human periosteum tissue. Scale bar = 50 μM. $n = 3$ human samples per group for transcriptomic and histologic data.

averaging of 6. Scan resolution was 9 μM. After imaging, the scan projections were reconstructed using the NRecon software (Bruker). Further analysis software including CTVox and CTAn (Bruker) was employed to analyze 3D morphometry, bone volume, and ratio of bone volume to total volume. Analysis thickness for each sample was 0.34 mm, with a rectangular region of interest (1500 mm to 1200 mm) with a threshold range of 40-90.

Histology and Immunohistochemistry

Samples after microCT were then transferred to 14% (w/v) ethylenediaminetetraacetic acid (EDTA) solution for 1 month. Samples were then immersed in 30% (w/v) sucrose and embedded in optimum cutting temperature solution. Sections of 10-μM thick were captured on glass slides and stained with Hematoxylin and Eosin (H&E). Sections were also treated with alkaline phosphatase staining kit (Sigma Aldrich, USA) for assessing enzymatic activity using previously published protocol.[13] ALP staining on sections was quantified using Image J software (NIH, USA). Immunofluorescence staining for osteocalcin (OCN, 1:100) and human nuclear antigen (HuNu,1:200) on sections was performed as mentioned above. Images were collected on a confocal laser scanning microscope (Zeiss LSM900). Fluorescence intensity within the implant site was quantified using Image J software (NIH, USA).

Statistical Analysis

Statistical analyses were performed in GraphPad Software 9.0. Quantitative data were expressed as mean ± 1SD. Statistical differences were analyzed by either Student's *t* test, or one-way or two-way analysis of variance with multiple comparisons. When needed, Welch's correction was applied. $^*P < .05$, $^{**}P < .01$, and $^{***}P < .001$ were considered significant unless otherwise stated within the figure legend.

Results

ZIC1 Is Highly Expressed in Adipose Tissue-Derived Human Mesenchymal Progenitor Cells

To identify TFs which regulate osteogenic/adipogenic cell differentiation within human mesenchymal progenitors, microarray was analyzed comparing adipose- versus skeletal-CD146^{+}Lin^{-} human pericytes (Fig. 1A).[15] Volcano plot and heat map representations showed several TFs highly expressed among adipose tissue-derived pericytes such as *HOXC10*, *MEIS2*, *SIM1*, and *ZIC1* (Fig. 1A, 1B). Of these, *ZIC1* was chosen for further analysis as prior studies have implicated the role of *ZIC1* TF in skeletal development and disease.[27-29] Sections of human adipose and bone tissue were analyzed for ZIC1 expression by immunofluorescence staining (Fig. 1C, 1D). The pericyte marker CD146 and endothelial marker CD31 were co-stained. Results confirmed differential ZIC1 expression, with a high degree of co-localization of ZIC1 and CD146 immunoreactivities within adipose tissue blood vessels (Fig. 1C). In contrast, very little ZIC1 immunoreactivity was found within skeletal/periosteal blood vessels (Fig. 1D). These data suggest that *ZIC1* is preferably expressed in adipose as compared with skeletal perivascular progenitor cells, despite its known functions in mature osteoblasts and osteocytes.[32,33]

ZIC1 Knockdown Enhances Adipogenesis Over Osteogenesis in Human Adipose-Derived Mesenchymal Progenitor Cells

ZIC1 expression was evaluated over the time course of adipogenic and osteogenic differentiation of human adipose-derived mesenchymal progenitor cells (hASCs, Fig. 2A). Results showed increased *ZIC1* expression at day 3 and 7 of adipogenesis, which decreased toward baseline by day 14 (Fig. 2A, red line). In contrast, *ZIC1* expression remained relatively constant over time during osteogenic differentiation (Fig. 2A, blue line). Effects of *ZIC1* knockdown in adipose-derived mesenchymal progenitor cells was next determined. Knockdown efficiency (*ZIC1* KD) was calculated by qRT-PCR and 60% knockdown compared to scramble siRNA was determined (Fig. 2B). Western blot analysis confirmed 55.5% reduction in expression of the ZIC1 protein with gene knockdown in comparison to control (Fig. 2C, Supplementary Fig. S2A). MTS assays showed no difference in cell proliferation between *ZIC1* KD and scramble siRNA-treated cells over 48 hours (Fig. 2D).

ZIC1 KD cells were next subjected to adipogenic differentiation. Oil red O staining and quantification of *ZIC1* KD and scramble siRNA showed an increase in oil vacuole accumulation among knockdown cells (Fig. 2E, 2F). Gene expression also increased with adipogenic differentiation upon *ZIC1* KD, including increased expression of peroxisome proliferator-activated receptor gamma (*PPARγ*), CCAAT/enhancer-binding protein alpha (*CEBPα*), and fatty acid-binding protein 4 (*FABP4*) (Fig. 2G, 36% [*PPARγ*], 14% [*CEBPα* and *FABP4*] increase in comparison to SiRNA control).

Next, the osteogenic differentiation potential of *ZIC1* KD cells was analyzed. After 10 days of osteogenesis, both knockdown and scramble siRNA-treated cells are stained for alkaline phosphatase (ALP) and alizarin red S (ARS). Overall, osteogenic differentiation among *ZIC1* KD cells was reduced as compared to scramble siRNA controls (Fig. 2H). Quantitative analysis of AR staining confirmed reduced mineralization among *ZIC1* KD cells (Fig. 2I, 50% reduction). Furthermore, osteogenesis-related gene expression showed a relative reduction in several genes among *ZIC1* siRNA-treated cells, including alkaline phosphatase (*ALPL*), Runt-like TF 2 (*RUNX2*), collagen 1 alpha 1 (*COL1A1*), osterix (*SP7*), and osteocalcin (*OCN*) (Fig. 2J, ranging from 12%-48% reduction in comparison to control). These data demonstrate that knocking down *ZIC1* expression favored adipogenesis over osteogenesis in human mesenchymal progenitor cells.

ZIC1 Overexpression Alters Hedgehog Signaling and Enhances Osteogenesis of Human Adipose-Derived Mesenchymal Progenitor Cells

To further investigate the regulatory effect of *ZIC1* on differentiation, ZIC was overexpressed in mesenchymal progenitors. *ZIC1* was overexpressed using a CMV plasmid (*ZIC1* OE). An empty lentiviral vector plasmid acted as control for *ZIC1* plasmid overexpression (LV). The overexpression efficiency of the *ZIC1* plasmid was confirmed by qPCR, demonstrating a 40% increase in expression (Fig. 3A). Western blot analysis confirmed increased ZIC1 protein expression in the overexpression group in comparison to control (Fig. 3B, Supplementary Fig. S2B). No significant difference in cell proliferation was observed between *ZIC1* OE and empty vector control (VC) (Fig. 3C).

The effect of *ZIC1* overexpression on osteogenic and adipogenic differentiation was next investigated. Oil red O staining and quantification showed decreased lipid droplet accumulation among *ZIC1* overexpressing cells (Fig. 3D, 3E). Adipogenesis gene expression confirmed a significant reduction in adipogenic differentiation among *ZIC1* OE cells (20%-45% reduction in comparison to LV) (Fig. 3F). Conversely, increased mineralization and ALP activity were observed among cells overexpressing *ZIC1* (Fig. 3G). Mineralization quantified from Alizarin red S staining showed a 30% increase among *ZIC1* overexpressing cells (Fig. 3G, 3H). In agreement with these findings, qRT-PCR analysis showed a significant upregulation of osteogenesis gene expression, including *RUNX2*, *ALPL*, *COL1α1*, *SP7*, and *OCN* within the *ZIC1* OE group (13%-47% increase in comparison to LV at day 10 of differentiation) (Fig. 3I). Thus, *ZIC1* overexpression favors osteogenesis over adipogenesis in human mesenchymal progenitor cells.

Osteogenic/anti-adipocytic effects of *ZIC1* overexpression closely mirrored those of Hedgehog signaling,[5] and *ZIC1* is known to interact with *GLI* TFs in other cell types.[34] We next analyzed the expression of Hedgehog pathway associated genes after *ZIC1* overexpression. After 48 hours of overexpression, qRT-PCR showed an 80% increase in sonic Hedgehog (*SHH*) expression. *SHH* upregulation was associated with increased expression of downstream target genes, including *PTCH1* (63% increase) and *GLI3* (12% increase) (Fig. 3J). Immunocytochemical staining showed GLI3 colocalizing with the ZIC1 in overexpression group (Fig. 3K). Overall, these results demonstrate that *ZIC1* overexpression promote osteogenic rather than adipogenic differentiation of adipose-derived human mesenchymal progenitor cells, which was associated with increased Hedgehog signaling.

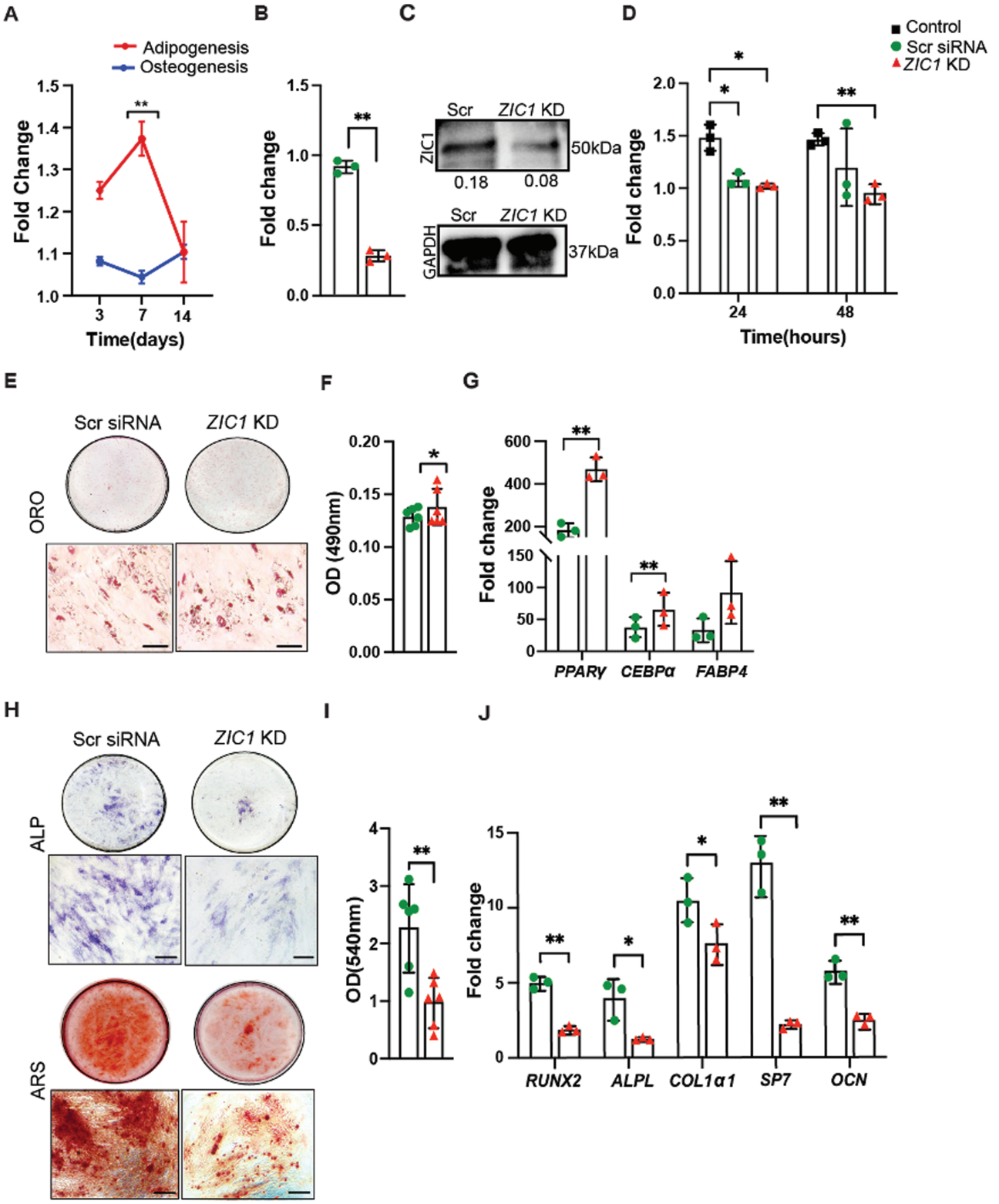

Figure 2. *ZIC1* knockdown in human adipose-derived mesenchymal progenitors increases adipogenesis. (**A**) Basal *ZIC1* expression over days of differentiation during adipogenesis (red) and osteogenesis (blue). (**B**) *ZIC1* knockdown (*ZIC1* KD) efficiency compared with scrambled siRNA (Scr siRNA). (**C**) Western blot of ZIC1 in knockdown cells compared with scramble siRNA, normalized to GAPDH. Uncropped version of western blot is given in Supplementary Fig. S2A. (**D**) MTS—cell proliferation assay over 24 hours and 48 hours. (**E**) Adipogenesis by Oil red O (ORO) staining at day 10 of differentiation—cell culture plate scan and bright field imaging. (**F**) Spectrophotometric quantification of Oil red O. (**G**) Adipogenesis-related genes by qRT-PCR at day 10 of differentiation. (**H**) Osteogenic differentiation by alkaline phosphatase (ALP) (d 7) and Alizarin red staining (ARS) (d 10). (**I**) Spectrophotometric quantification of Alizarin red staining. (**J**) Osteogenesis-related genes by qRT-PCR at day 10 of differentiation. **P*<.05, ***P*<.01. *n = 3* biological replicates for *in vitro* assays. Scale bar = 50 μM. Mean and 1 SD are shown, with individual data points reflecting individual measurements.

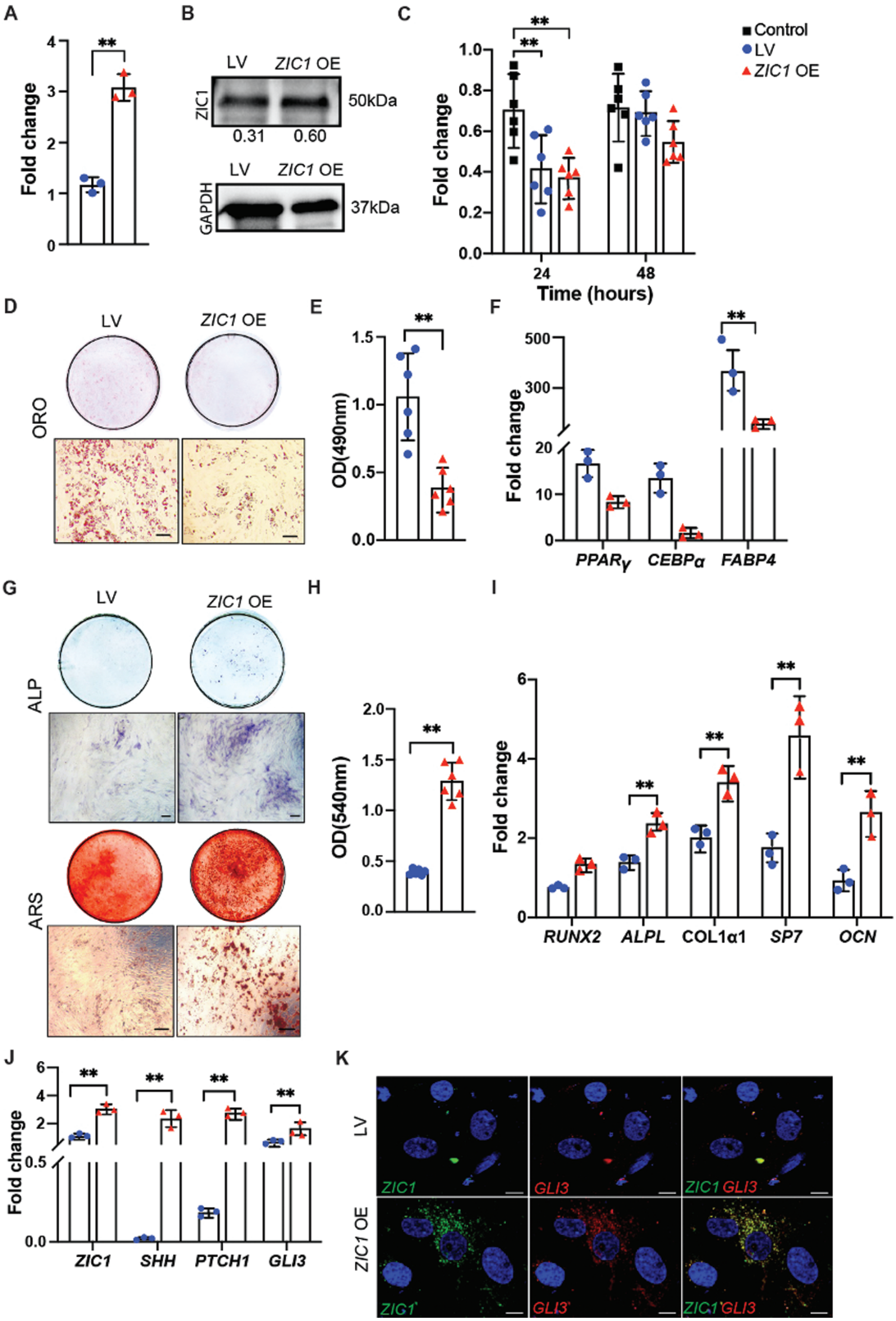

Figure 3. *ZIC1* overexpression induces osteogenesis and inhibits adipogenesis among human adipose-derived mesenchymal progenitor cells. (**A**) Overexpression efficiency of *ZIC1* in adipose-derived mesenchymal progenitor cells (hASCs). (**B**) Western blot of ZIC1 in *ZIC1* OE compared with empty lentiviral control, normalized to GAPDH. Uncropped version of western blot is given in Supplementary Fig. S2B. (**C**) MTS cell proliferation at 24 hours and 48 hours. (**D**) Adipogenesis assessed by Oil red O staining at day 10 of differentiation. Whole well and microscopic images shown and brightfield images. (**E**) Oil red O spectrophotometric quantification. (**F**) Adipogenesis-related gene expression by qRT-PCR at 10 days of differentiation, including *PPARγ*, *CEBPα*, and *FABP4*. (**G**) Alkaline phosphatase and Alizarin red S (ARS) staining at days 7 and 10 of osteogenic differentiation, respectively. Whole well and microscopic images shown. (**H**) ARS spectrophotometric quantification. (**I**) Osteogenesis-related gene expression by qRT-PCR at 10 days of differentiation, including *RUNX2*, *ALPL*, *COL1α1*, *SP7*, and *OCN*. (**J**) Sonic Hedgehog signaling associated gene expression, including *SHH, PTCH1*, and *GLI3* at day 2 of overexpression. (**K**) Immunofluorescent staining for ZIC1 (green) and GLI3 (red) with or without *ZIC1* overexpression. **P*<.05, ***P*<.01. *n* = 3 biological replicates for *in vitro* assays. Scale bar = 50 μM (black) and 20 μM (white). Mean and 1 SD are shown, with individual data points reflecting individual measurements.

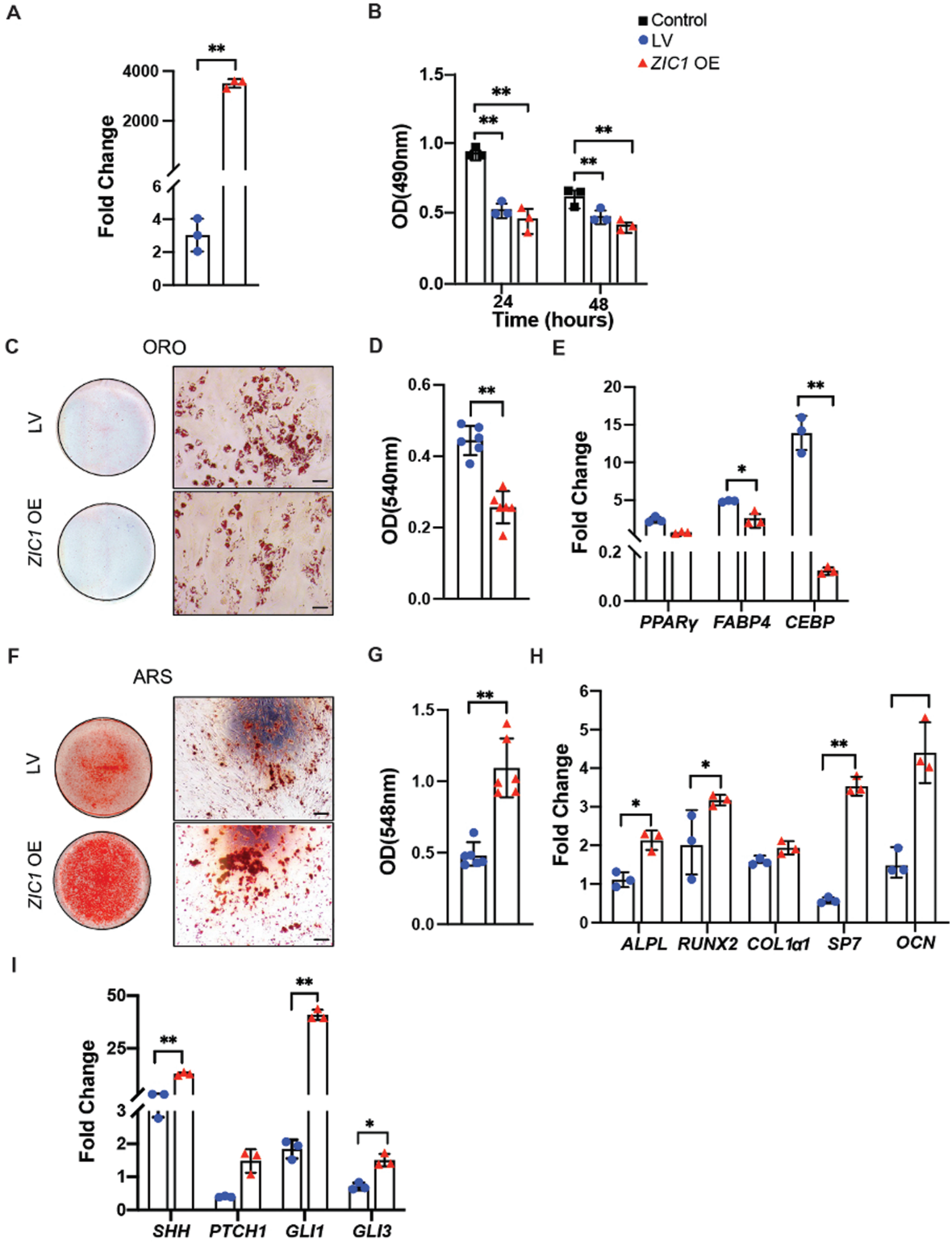

Figure 4. *ZIC1* overexpression in adipose-derived pericytes increases osteogenesis. (**A**) Overexpression efficiency of *ZIC1* in human pericytes. (**B**) MTS cell proliferation assay at 24 hours and 48 hours. (**C**) Oil red O staining at day 10 of adipogenic differentiation, whole well images and microscopic images shown. (**D**) Oil red O spectrophotometric quantification. (**E**) Adipogenesis-related gene expression by qRT-PCR at 10 days of differentiation, including *PPARγ*, *FABP4*, and *CEBPα*. (**F**) Alizarin red S (ARS) staining at day 10 of osteogenic differentiation. Whole well images and microscopic images shown. (**G**) ARS spectrophotometric quantification. (**H**) Osteogenesis-related gene expression by qRT-PCR at 10 days of differentiation, *ALPL, RUNX2, COL1α1, SP7*, and *OCN*. (**I**) Sonic Hedgehog signaling-related genes, including *SHH, PTCH1, GLI1*, and *GLI3*. **P*<.05, ***P*<.01. *n* = 3 biological replicates for *in vitro* assays. Mean and 1 SD are shown, with individual data points reflecting individual measurements.

ZIC1 Overexpression Enhances Osteogenesis in Human Adipose-Derived Pericytes and a Human Osteosarcoma Cell Line

Given the strong effects of *ZIC1* overexpression on the osteo/adipogenic differentiation of culture-derived human mesenchymal progenitor cells, we performed follow-up studies on human purified pericytes, which include native MSC forerunners,[1] as well as osteoblastic cell lines like Saos-2. First, *ZIC1* was overexpressed in human adipose-derived CD146$^+$ pericytes (Supplementary Fig. S1 for cell isolation). Resulting expression of *ZIC1* was 1200-fold higher, compared to an empty lentiviral vector control (Fig. 4A). Pericyte proliferation was not significantly different between the overexpression group and the lentiviral vector group, compared to an untreated control group after 48 hours (Fig. 4B).

Changes in adipo- and osteogenic differentiation in human pericytes overexpressing *ZIC1* largely mirrored changes observed in similarly modified hASCs. In pericytes overexpressing *ZIC1*, adipogenesis decreased (48.7%), as shown by Oil red O staining and quantification after 10 days of differentiation (Fig. 4C, 4D), accompanied by a reduction in adipogenesis marker gene expression (up to 67% decrease in comparison to LV, Fig. 4E). Conversely, *ZIC1* overexpression in human pericytes increased mineralization as revealed by Alizarin red staining (34% increase in *ZIC1* OE) and quantification at day 10 after osteogenic induction (Fig. 4F, 4G), and osteogenesis marker gene expression at 10 day of differentiation (up to 47% increase in comparison to vector control, Fig. 4H). Hedgehog signaling showed a similar trend in human pericytes with *ZIC1* overexpression, including an increase in transcripts of *SHH* (67%), *PTCH1* (23%), *GLI1* (86%), and *GLI3* (18%) in comparison to vector control (Fig. 4I).

As the pro-osteogenic effects of *ZIC1* overexpression were prominent, we sought to confirm this in the osteoblastic cell line Saos-2 (Supplementary Fig. S3). After confirming *ZIC1* overexpression (Supplementary Fig. S2A), a slight reduction in cell proliferation was observed in comparison to vector control (Supplementary Fig. S2B). As in other cell types, *ZIC1* overexpression resulted in increased bone nodule formation at day 7 (Supplementary Fig. S2C), and a significant increase in osteogenesis gene expression at day 7 (Supplementary Fig. S2D). Similarly, genes in the Hedgehog signaling pathway showed an increased expression among *ZIC1* overexpressing Saos-2 cells, including *SHH* itself (Supplementary Fig. S2E). These data confirmed conserved effects of overexpression of the TF *ZIC1* across human progenitor cell types as well as human cell lines.

The Hedgehog Antagonist Cyclopamine Reverses *ZIC1*-Mediated Changes in Differentiation in Adipose-Derived Mesenchymal Progenitor Cells

Next, the effects of the Hedgehog signaling antagonist cyclopamine were tested in the context of *ZIC1* overexpression in human mesenchymal progenitor cells. During osteogenic differentiation, *ZIC1* overexpression resulted in an increase in mineralization, which was completely abrogated by the addition of cyclopamine to the osteogenic differentiation medium (Fig. 5A). Similar results were observed by qRT-PCR with osteogenesis gene expression (Fig. 5B). Cyclopamine alone consistently reduced osteogenesis gene expression, while *ZIC1* overexpression alone consistently increased osteogenesis gene expression. Furthermore, cyclopamine treatment completely reversed the pro-osteogenic effects of *ZIC1* overexpression across all genes examined (Fig. 5B).

Cyclopamine treatment also demonstrated significant effects on the adipogenic potential of *ZIC1* overexpressing progenitor cells. In agreement with our prior observations, *ZIC1* overexpression led to a significant reduction in adipogenic differentiation, according to Oil red O staining (Fig. 5C) and adipogenesis gene expression (Fig. 5D). Interestingly, cyclopamine treatment partially or fully restored the adipogenic differentiation of *ZIC1* overexpressing cells to levels of vector control (Fig. 5C). Thus, osteo/adipogenic differentiation changes mediated by *ZIC1* can be reversed by modulation of Hedgehog signaling.

ZIC1 Overexpression Induces Increased Bone Formation *In Vivo*

To further test their osteogenic potential, hASCs overexpressing *ZIC1* or VC were implanted subcutaneously into NOD-SCID *gamma* mice using a HA/β-TCP scaffold. Cells treated with empty lentiviral vector served as control. Six mice were operated, each receiving 2 implants (Fig. 6A). X-ray images showed the intact nature of implanted ossicle at 12 weeks, with no change in implant position across samples (Supplementary Fig. S4). DEXA analysis showed a progressive increase in bone mineral density in the *ZIC1* overexpression group compared to the empty lentiviral group over 12 weeks of growth (Fig. 6B). MicroCT analysis showed a qualitative increase in tissue density among *ZIC1* overexpressing implants (Fig. 6C), with quantitative analysis showing increased bone volume and bone volume/total volume ratio (Fig. 6D, 6E). H&E (Fig. 6F) and alkaline phosphatase staining showed increased staining intensity in the *ZIC1* overexpression group (Fig. 6G). Similarly, co-immunostaining of osteocalcin (OCN) and human nuclear antigen (HuNu) showed increased OCN expression in the *ZIC1* OE group compared to the lentiviral control in and around areas of HuNu positivity (Fig. 6H, 6I). Overall, these results demonstrate that induced expression of the TF *ZIC1* in human mesenchymal progenitors led to significant increases in subcutaneous ossicle formation.

Discussion

Identification of novel TFs regulating lineage commitment of mesenchymal progenitor cells is necessary to understand niche-specific regeneration attributes. In this study, we identified *Z1C1*, among other TFs, differentially expressed between pericytes in different human organs. *ZIC1* was in turn found to repress adipogenesis and promote osteogenesis among mesenchymal progenitor cells, including pericytes, and do so through a Hedgehog signaling-dependent mechanism.

The *ZIC* family of zinc finger TFs exhibit major roles during early development. They are critical during neural tube formation, musculoskeletal development, patterning, and morphogenesis.[27-29,35] Even though the early developmental/functional activities of distinct *ZIC* genes overlap, several studies indicate that mutation of each *ZIC* gene leads to exclusive aberrant phenotypes. For example, *ZIC1* global gene deletion in mice results in axial skeletal malformations and cerebellar defects.[36,37] *In vitro*, *ZIC* expression showed a correlation with mechanosensory regulation of osteogenic activity. In the above study, *ZIC1* anabolically regulated bone formation by osteoblasts and osteocytes in response to

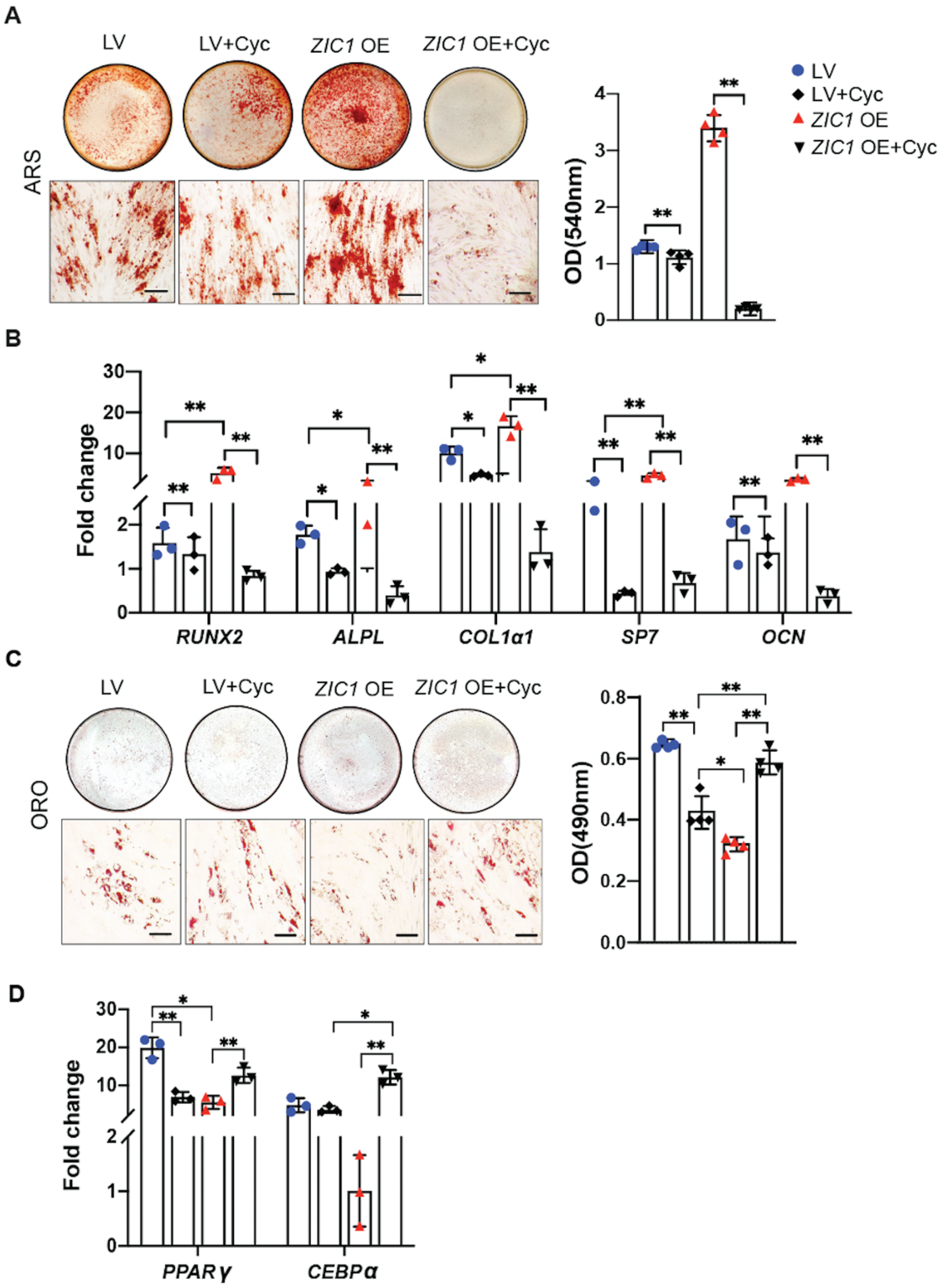

Figure 5. Effect of Hh signaling antagonism on the differentiation of mesenchymal progenitor cells with *ZIC1* overexpression. Human ASCs with *ZIC1* overexpression (OE) or lentiviral vector control (LV) were exposed to differentiation conditions with or without cyclopamine (Cyc, 5 μM). (**A**) Alizarin red staining (left) and spectrophotometric quantification (right) after 10 days of osteogenic differentiation. Whole well and microscopic images shown. (**B**) Osteogenic-related gene expression by qRT-PCR at day 10 of differentiation, including *RUNX2*, *ALP*, *COL1α1*, *SP7*, and *OCN*. (**C**) Oil red O staining (left) and quantification (right) at day 10 of adipogenic differentiation. Whole well and microscopic images shown. (**D**) Adipogenesis-related gene expression by qRT-PCR at day 10 of differentiation, including *PPARγ*, *CEBPα*. **P*<.05, ***P*<.01. *n* = 3 biological replicates for *in vitro* assays. Scale bar = 50 μm. Mean and 1 SD are shown, with individual datapoints reflecting individual measurements.

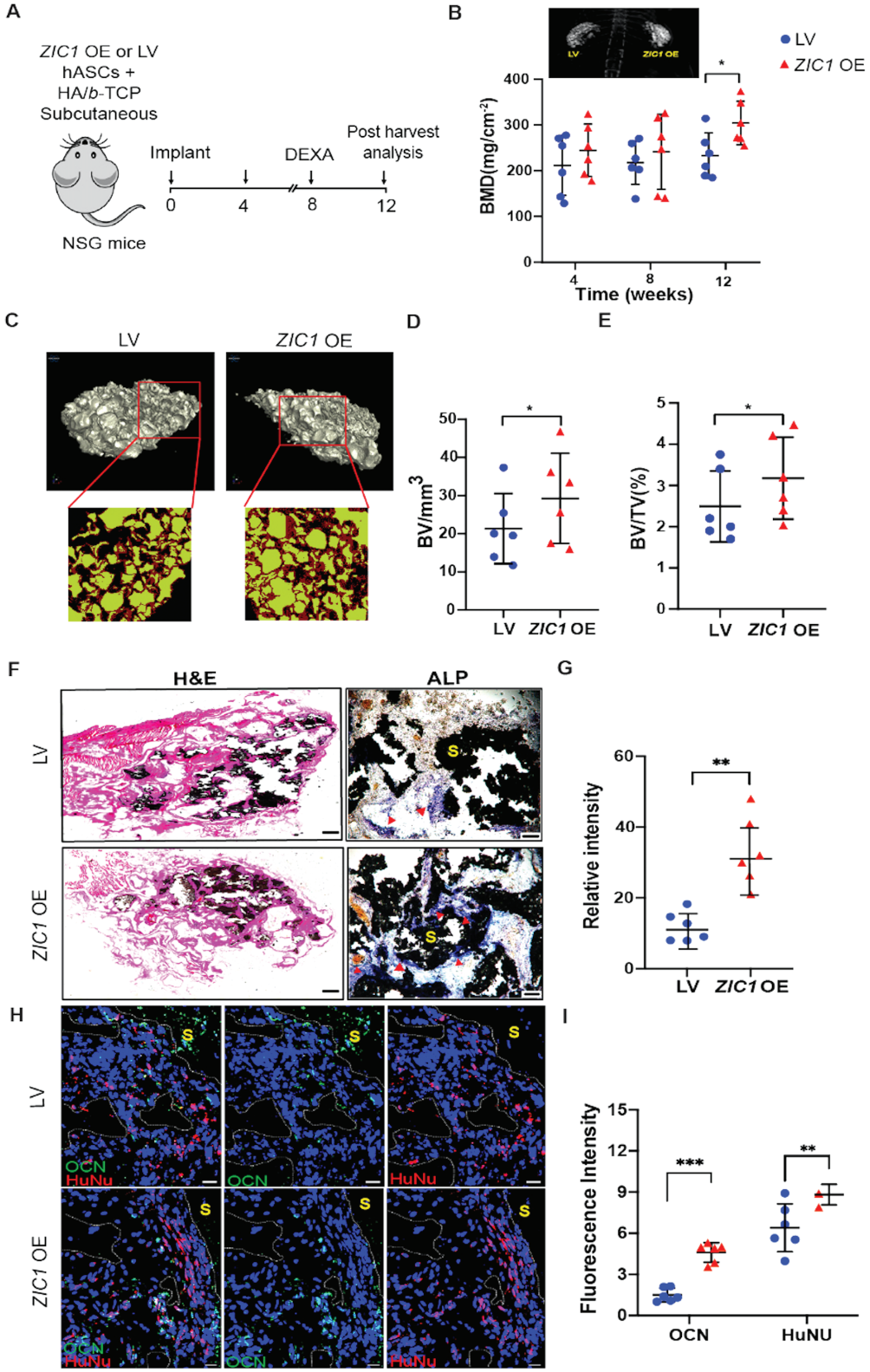

Figure 6. *ZIC1* overexpression enhances human ASC-mediated ectopic bone formation. (**A**) Schematics of ossicle implantation in NOD-SCID *gamma* mice and time course of analyses. (**B**) Bone mineral density of *ZIC1* OE compared with LV control at 4, 8, and 12 weeks, by DEXA analysis. Representative cropped image of implant appearance by DEXA (above). (**C**) Representative microCT 3D reconstructions of ossicles. Inset shows pseudo-colored density difference of new bone tissue formed and HA/β-TCP scaffold implant (scaffold: green, tissue: red, background: black). (**D**) Bone volume (BV) and (**E**) bone volume to total volume (BV/TV) as assessed by microCT at 12 weeks postimplantation. (**F**) Representative histologic appearance of implants by H&E staining and representative ALP staining (dark colored scaffold labeled S in yellow, ALP positive: red arrows). (**G**) Quantification of new bone area through relative intensity of ALP staining. (**H**) Panel for immunofluorescent staining of osteocalcin (OCN, red) and human-specific nuclei (HuNu, green) within implants (white dashed lines demarcated the edges of the scaffold and scaffold area labeled as S in yellow). (**I**) Relative fluorescence intensity of OCN and HuNu. Mean and 1 SD are shown, with individual animal measurements indicated. **P*<.05, ***P*<.01, ****P*<.001. *n* = 6 animals per group. Scale bar = 50 μM (histology). Scale bar = 20 μM (immunofluorescence).

mechanical loading and microfracture.[28,37] These studies indicate that the *ZIC1* gene has significant and to some extent underexplored roles in the regulation of osteogenic activity.

The zinc finger domain of the *ZIC* family shares similarities with GLI family ZF domains.[34,38] Several investigations observe that ZIC proteins physically interact with GLI proteins *in vitro*, leading to hypothesize that they interact or compete with GLI family TFs to regulate Hh signaling.[29,34,37-40] Our previous studies show that Hedgehog signaling supports the differentiation of mesodermal multipotent cells to the osteogenic lineage by suppressing adipogenesis.[39] In the present work, *ZIC1* appears to positively regulate Hh signaling, including an increased expression of the Hh signaling target genes *Gli1* and *Ptch1*, which was correlated with osteogenic induction. The reversal of *ZIC1* overexpression-mediated osteogenesis after cyclopamine treatment (Hedgehog antagonist) suggests an upstream role of *ZIC1* in Hedgehog signaling.[33,38,41] In agreement, a recent report indicated that ZIC1 mediates shear stress-induced mechanotransduction in murine osteocytes through both Wnt/β-catenin and Hedgehog signaling.[42] In another context, *ZIC1* was identified as a key marker in brain pericyte-like cells generated from neural crest stem cells derived from human pluripotent stem cells.[43] The pathway regulation was by Wnt activation and inhibition of TGFb/BMP signaling for *ZIC1* in brain pericyte-like cells.[43-45] *ZIC1* is also extensively studied in cancer disease progression, where it appears to predominantly act as a tumor suppressor through regulation of Sonic Hedgehog, PI3K, and MAPK signaling.[45] Thus, the pro-osteogenic effect of *ZIC1* as observed in human mesenchymal progenitor cells here may occur via changes in a confluence of signaling pathways, including Hh signaling.

*ZIC*1 has been reported as a marker of brown adipogenesis. It has, indeed, a suggestive role in brown adipocyte precursor differentiation and white to brown adipocyte transdifferentiation.[46-48] In agreement, we observed in preliminary analyses that brown adipogenesis markers are strongly upregulated with *ZIC1* overexpression (data not shown). It is interesting to note that several studies indicate that Hedgehog signaling inhibits brown adipose tissue formation.[48-50] Therefore, it is likely that the possible effects of *ZIC1* on brown adipose differentiation are independent of Hh, while the influence of *ZIC1* on white adipogenesis is Hh signaling dependent.[47,50] Importantly, a body of studies have examined the paracrine or endocrine interactions between brown adipocytes and osteoblasts.[48-51] Although we did identify upregulation of *UCP1* and *CIDEA* during osteogenesis among *ZIC1* overexpressing cells, we were not able to localize definitive brown adipocytes in any of the sections of the experimental ossicles. The role of *ZIC1*-induced changes in brown adiposity may not directly correlate with the osteogenesis observed among mesenchymal progenitors in the present study and require further investigation.

In summary, the *ZIC1* gene is differentially expressed in human adipose progenitor cells compared with skeletal progenitors. Forced overexpression of the *ZIC1* TF in human adipose-derived mesenchymal progenitor cells favored osteogenesis, both *in vitro* and *in vivo,* via a Hedgehog-dependent mechanism. Thus, the *ZIC1* TF is an active modulator of mesenchymal progenitor osteogenesis at the expense of adipogenesis, a property that could be further explored for bone regeneration therapies.

Acknowledgments

The content is solely the responsibility of the authors and does not necessarily represent the official views of the National Institute of Health or Department of Defense. We thank JHU-microscopic facility, deep sequencing, and microarray facility, animal care facility, and Hao Zhang of Bloomberg flow cytometry facility for the assistance provided.

Funding

A.W.J. was funded by NIH/NIAMS (R01 AR070773, R01 AR068316), USAMRAA through the Peer Reviewed Medical Research Program (W81XWH-18-1-0121, W81XWH-18-1-0336), Peer Reviewed Orthopaedic Research Program (W81XWH-20-10795) and Broad Agency Announcement (W81XWH-18-10613), and the Maryland Stem Cell Research Foundation.

Conflict of Interest

A.W.J. declared scientific advisory board for Novadip LLC, consultant for Lifesprout LLC and Novadip LLC, and Editorial Board of Bone Research, American Journal of Pathology. K.B. declared consultant for Dilon Technologies. All of the other authors declared no potential conflicts of interest.

Author Contributions

Conception and design, collection, assembly of data, data analysis and interpretation, manuscript writing: N.T. Collection, data analysis and interpretation, manuscript writing: M.G.-S. Collection, data analysis and interpretation: M.X. Collection, assembly of data, data analysis and interpretation: Q.Q. Data analysis and interpretation: X.X., J.X., J.-H.Y. Provision of study material: K.B. Collection of data and study material: M.A. Conception and design, collection, assembly of data, analysis, and interpretation: G.C.-Y.H. Conception and design, manuscript writing: B.P. Conception and design, collection, assembly of data, data analysis and interpretation, manuscript writing, provision of study material, financial support, final approval of manuscript: A.W.J.

Data Availability

The data that supports the findings of this study are available within the article and its supplementary data files.

Supplementary Material

Supplementary material is available at *Stem Cells* online.

References

1. Crisan M, Yap S, Casteilla L, et al. A perivascular origin for mesenchymal stem cells in multiple human organs. *Cell Stem Cell*. 2008;3(3):301-313. https://doi.org/10.1016/j.stem.2008.07.003.
2. Anghileri E, Marconi S, Pignatelli A, et al. Neuronal differentiation potential of human adipose-derived mesenchymal stem cells. *Stem Cells Dev*. 2008;17(5):909-916. https://doi.org/10.1089/scd.2007.0197.

3. Gimble JM, Guilak F. Adipose-derived adult stem cells: isolation, characterization, and differentiation potential. *Cytotherapy*. 2003;5(5):362-369. https://doi.org/10.1080/14653240310003026.
4. Pittenger MF, Mackay AM, Beck SC, et al. Multilineage potential of adult human mesenchymal stem cells. *Science*. 1999;284(5411):143-147. https://doi.org/10.1126/science.284.5411.143.
5. James AW. Review of signaling pathways governing MSC osteogenic and adipogenic differentiation. *Scientifica*. 2013;2013(12):1-17. https://doi.org/10.1155/2013/684736
6. Mitxitorena I, Infante A, Gener B, Rodríguez CI. Suitability and limitations of mesenchymal stem cells to elucidate human bone illness. *World J Stem Cells*. 2019;11(9):578-593. https://doi.org/10.4252/wjsc.v11.i9.578.
7. James AW, Péault B. Perivascular mesenchymal progenitors for bone regeneration. *J Orthop Res*. 2019;37(6):1221-1228. https://doi.org/10.1002/jor.24284.
8. Xu J, Wang Y, Gomez-Salazar MA, et al. Bone-forming perivascular cells: cellular heterogeneity and use for tissue repair. *Stem Cells*. 2021;39(11):1427-1434. https://doi.org/10.1002/stem.3436.
9. Meyers CA, Wang C, Xu J, et al. Assessing the bone-forming potential of pericytes. *Methods Mol Biol*. 2021;2235:127-137. https://doi.org/10.1007/978-1-0716-1056-5_9.
10. Negri S, Wang Y, Sono T, et al. Human perivascular stem cells prevent bone graft resorption in osteoporotic contexts by inhibiting osteoclast formation. *Stem Cells Transl Med*. 2020;9(12):1617-1630. https://doi.org/10.1002/sctm.20-0152.
11. Wang Y, Xu J, Chang L, et al. Relative contributions of adipose-resident CD146$^+$ pericytes and CD34$^+$ adventitial progenitor cells in bone tissue engineering. *NPJ Regen Med*. 2019;4(1):1.
12. Xu J, Wang Y, Hsu CY, et al. Lysosomal protein surface expression discriminates fat- from bone-forming human mesenchymal precursor cells. *Elife*. 2020;9:e58990. https://doi.org/10.7554/eLife.58990.
13. Wang Y, Xu J, Meyers CA, et al. PDGFRα marks distinct perivascular populations with different osteogenic potential within adipose tissue. *Stem Cells*. 2020;38(2):276-290. https://doi.org/10.1002/stem.3108.
14. Stefanska A, Kenyon C, Christian HC, et al. Human kidney pericytes produce renin. *Kidney Int*. 2016;90(6):1251-1261. https://doi.org/10.1016/j.kint.2016.07.035.
15. Xu J, Li D, Hsu CY, et al. Comparison of skeletal and soft tissue pericytes identifies CXCR4$^+$ bone forming mural cells in human tissues. *Bone Res*. 2020;8(1):22. https://doi.org/10.1038/s41413-020-0097-0.
16. Wang Y, Negri S, Li Z, et al. Anti-DKK1 enhances the early osteogenic differentiation of human adipose-derived stem/stromal cells. *Stem Cells Dev*. 2020;29(15):1007-1015. https://doi.org/10.1089/scd.2020.0070.
17. Negri S, Wang Y, Sono T, et al. Systemic DKK1 neutralization enhances human adipose-derived stem cell mediated bone repair. *Stem Cells Transl Med*. 2021;10(4):610-622. https://doi.org/10.1002/sctm.20-0293.
18. Meyers CA, Xu J, Asatrian G, et al. WISP-1 drives bone formation at the expense of fat formation in human perivascular stem cells. *Sci Rep*. 2018;8(1):15618. https://doi.org/10.1038/s41598-018-34143-x.
19. Lu GM, Rong YX, Liang ZJ, et al. Multiomics global landscape of stemness-related gene clusters in adipose-derived mesenchymal stem cells. *Stem Cell Res Ther*. 2020;11(1):310. https://doi.org/10.1186/s13287-020-01823-3.
20. Robert AW, Angulski ABB, Spangenberg L, et al. Gene expression analysis of human adipose tissue-derived stem cells during the initial steps of in vitro osteogenesis. *Sci Rep*. 2018;8(1):4739. https://doi.org/10.1038/s41598-018-22991-6.
21. Kurenkova AD, Medvedeva EV, Newton PT, Chagin AS. Niches for skeletal stem cells of mesenchymal origin. *Front Cell Dev Biol*. 2020;8:592. https://doi.org/10.3389/fcell.2020.00592.
22. Li S, Xue T, He F, et al. A time-resolved proteomic analysis of transcription factors regulating adipogenesis of human adipose derived stem cells. *BBRC*. 2019;511(4):855-861. https://doi.org/10.1016/j.bbrc.2019.02.134.
23. Chen EEM, Zhang W, Ye CCY, et al. Knockdown of SIRT7 enhances the osteogenic differentiation of human bone marrow mesenchymal stem cells partly via activation of the Wnt/β-catenin signaling pathway. *Cell Death Dis*. 2017;8(9):e3042-e3042. https://doi.org/10.1038/cddis.2017.429.
24. Ye C, Chen M, Chen E, et al. Knockdown of FOXA2 enhances the osteogenic differentiation of bone marrow-derived mesenchymal stem cells partly via activation of the ERK signalling pathway. *Cell Death Dis*. 2018;9(8):1-13.
25. Iwata T, Kawamoto T, Sasabe E, et al. Effects of overexpression of basic helix-loop-helix transcription factor Dec1 on osteogenic and adipogenic differentiation of mesenchymal stem cells. *Eur J Cell Biol*. 2006;85(5):423-431. https://doi.org/10.1016/j.ejcb.2005.12.007.
26. Rauch A, Mandrup S. Transcriptional networks controlling stromal cell differentiation. *Nat Rev Mol Cell Biol*. 2021;22(7):465-482. https://doi.org/10.1038/s41580-021-00357-7.
27. Christa A. Mezedorf, emerging toles of ZIC genes in early development. *Dev Dyn*. 2007;236(4):922-940.
28. Datta HK, Kringen MK, Tuck SP, et al. Mechanical-stress-related epigenetic regulation of ZIC1 transcription factor in the etiology of postmenopausal osteoporosis. *Int J Mol Sci*. 2022;23(6):2957.
29. Kalogeropoulos M, Varanasi SS, Olstad OK, et al. Zic1 transcription factor in bone: neural development protein regulates mechanotransduction in osteocytes. *FASEB J*. 2010;24(8):2893-2903. https://doi.org/10.1096/fj.09-148908.
30. Bourin P, Bunnell AB, Casteilla L, et al. Stromal cells from the adipose tissue-derived stromal vascular fraction and culture expanded adipose tissue-derived stromal/stem cells: a joint statement of the International Federation for Adipose Therapeutics and Science (IFATS) and the International Society for Cellular Therapy (ISCT). *Cytotherapy*. 2013;15(6):641-648.
31. Qin Q, Gomez-Salazar M, Tower RJ, et al. NELL1 regulates the matrisome to promote osteosarcoma progression. *Cancer Res*. 2022;82(15):2734-2747. https://doi.org/10.1158/0008-5472.CAN-22-0732.
32. Suh JM, Gao X, McKay J, et al. Hedgehog signaling plays a conserved role in inhibiting fat formation. *Cell Metab*. 2006;3(1):25-34. https://doi.org/10.1016/j.cmet.2005.11.012.
33. Cousin W, Fontaine C, Dani C, Peraldi P. Hedgehog and adipogenesis: fat and fiction. *Biochimie*. 2007;89(12):1447-1453. https://doi.org/10.1016/j.biochi.2007.08.012.
34. Aruga J, Kamiya A, Takahashi H, et al. A wide-range phylogenetic analysis of Zic proteins: implications for correlations between protein structure conservation and body plan complexity. *Genomics*. 2006;87(6):783-792. https://doi.org/10.1016/j.ygeno.2006.02.011.
35. Houtmeyers R, Souopgui J, Tejpar S, Arkell R. The ZIC gene family encodes multi-functional proteins essential for patterning and morphogenesis. *Cell Mol Life Sci*. 2013;70(20):3791-3811. https://doi.org/10.1007/s00018-013-1285-5.
36. Twigg SRF, Forecki J, Goos JAC, et al. Gain-of-function mutations in ZIC1 are associated with coronal craniosynostosis and learning disability. *Am J Hum Genet*. 2015;97(3):378-388. https://doi.org/10.1016/j.ajhg.2015.07.007.
37. Ahmed JN, Diamand KEM, Bellchambers HM, Arkell RM. Systematized reporter assays reveal ZIC protein regulatory abilities are subclass-specific and dependent upon transcription factor binding site context. *Sci Rep*. 2020;10(1):13130. https://doi.org/10.1038/s41598-020-69917-9.
38. Aruga J, Mizugishi K, Koseki H, et al. Zic1 regulates the patterning of vertebral arches in cooperation with Gli3. *Mech Dev*. 1999;89(1(2):141-150.
39. James AW, Leucht P, Levi B, et al. Sonic Hedgehog influences the balance of osteogenesis and adipogenesis in mouse adipose-derived stromal cells. *Tissue Eng Part A*. 2010;16(8):2605-2616. https://doi.org/10.1089/ten.TEA.2010.0048.
40. Zhang Y, Beachy PA. Cellular and molecular mechanisms of Hedgehog signalling. *Nat Rev Mol Cell Biol*. 2023.

41. Cousin W, Fontaine C, Peraldi P. Inhibition of the anti-adipogenic Hedgehog signaling pathway by cyclopamine does not trigger adipocyte differentiation. *BBRC* 2006;349(2):799-803.
42. Stebbins MJ, Gastfriend BD, Canfield SG, et al. Human pluripotent stem cell-derived brain pericyte-like cells induce blood-brain barrier properties. *Sci Adv*. 2019;5(3):eaau7375. https://doi.org/10.1126/sciadv.aau7375.
43. Jeske R, Albo J, Marzano M, Bejoy J, Li Y. Engineering brain-specific pericytes from human pluripotent stem cells. *Tissue Eng Part B Rev*. 2020;26(4):367-382. https://doi.org/10.1089/ten.TEB.2020.0091.
44. Merzdorf CS, Sive HL. The zic1 gene is an activator of Wnt signaling. *Int J Dev Biol*. 2006;50(7):611-617. https://doi.org/10.1387/ijdb.052110cm.
45. Zhong J, Chen S, Xue M, et al. ZIC1 modulates cell-cycle distributions and cell migration through regulation of sonic Hedgehog, PI_3K and MAPK signaling pathways in gastric cancer. *BMC Cancer* 2012;12:290. https://doi.org/10.1186/1471-2407-12-290.
46. Lidell M, Betz M, Leinhard O, et al. Evidence for two types of brown adipose tissue in humans. *Nat Med*. 2013;19:631-634.
47. Rockstroh D, Landgraf K, Wagner IV, et al. Direct evidence of brown adipocytes in different fat depots in children. *PLoS One*. 2015;10(2):e0117841. https://doi.org/10.1371/journal.pone.0117841.
48. Wei S, Zhang L, Zhou X, et al. Emerging roles of zinc finger proteins in regulating adipogenesis. *Cell Mol Life Sci*. 2013;70(23):4569-4584. https://doi.org/10.1007/s00018-013-1395-0.
49. Omsted-Davis E, Gannon FH, Ozen M, et al. Hypoxic adipocytes pattern early heterotopic bone formation. *Am J Pathol*. 2007;170(2):620-632.
50. Nosavanh L, Yu D-H, Jaehnig EJ, et al. Cell-autonomous activation of Hedgehog signaling inhibits brown adipose tissue development. *Proc Natl Acad Sci U S A*. 2015;112(16):5069-5074. https://doi.org/10.1073/pnas.1420978112.
51. Sima R, Lu Y, Piotr JC, et al. Inducible brown adipose tissue, or beige fat, is anabolic for the skeleton. *Endocrinology*. 2013;154(8):2687-2701.